


# Design and optimization of a laser-PIXE beamline for material science applications

A. Morabito<sup>1,2</sup> , M. Scisciò<sup>2,3</sup>, S. Veltri<sup>4</sup>, M. Migliorati<sup>2</sup> and P. Antici<sup>5</sup>

## Research Article

**Cite this article:** Morabito A, Scisciò M, Veltri S, Migliorati M, Antici P (2019). Design and optimization of a laser-PIXE beamline for material science applications. *Laser and Particle Beams* 1–10. <https://doi.org/10.1017/S0263034619000600>

Received: 11 June 2019

Revised: 1 August 2019

Accepted: 6 August 2019

### Key words:

Cultural heritage; hybrid beamline and beam manipulation; ion beam analysis; laser-driven proton acceleration; laser-PIXE; particle induced X-ray emission (PIXE)

**Author for correspondence:** A. Morabito, ELI-ALPS, ELI-HU Non profit Ltd., Dugonics ter 13, Szeged, 6720, Hungary.  
E-mail: [antonia.morabito@eli-alps.hu](mailto:antonia.morabito@eli-alps.hu)

<sup>1</sup>ELI-ALPS, ELI-HU Non profit Ltd., Dugonics ter 13, Szeged, 6720, Hungary; <sup>2</sup>INFN and University of Rome, Via Scarpa 14, 00161 Roma, Italy; <sup>3</sup>ENEA, Fusion and Nuclear Safety Department, C. R. Frascati, Via E. Fermi 45, Frascati, 00044 Roma, Italy; <sup>4</sup>Institute of Low Temperature and Structure Research, Polish Academy of Sciences, PL-50422 Wrocław, Poland and <sup>5</sup>INRS-EMT, 1650 Boul. Lionel Boulet, J3X 1S2, Varennes, Canada

### Abstract

Multi-MeV proton beams can be generated by irradiating thin solid foils with ultra-intense ( $>10^{18}$  W/cm<sup>2</sup>) short laser pulses. Several of their characteristics, such as high bunch charge and short pulse duration, make them a complementary alternative to conventional radio frequency-based accelerators. A potential material science application is the chemical analysis of cultural heritage (CH) artifacts. The complete chemistry of the bulk material (ceramics, metals) can be retrieved through sophisticated nuclear techniques such as particle-induced X-ray emission (PIXE). Recently, the use of laser-generated proton beams was introduced as diagnostics in material science (laser-PIXE or laser-driven PIXE): Coupling laser-generated proton sources to conventional beam steering devices successfully enhances the capture and transport of the laser-accelerated beam. This leads to a reduction of the high divergence and broad energy spread at the source. The design of our hybrid beamline is composed of an energy selector, followed by permanent quadrupole magnets aiming for better control and manipulation of the final proton beam parameters. This allows tailoring both, mean proton energy and spot sizes, yet keeping the system compact. We performed a theoretical study optimizing a beamline for laser-PIXE applications. Our design enables monochromatizing the beam and shaping its final spot size. We obtain spot sizes ranging between a fraction of mm up to cm scale at a fraction of nC proton charge per shot. These results pave the way for a versatile and tunable laser-PIXE at a multi-Hz repetition rate using modern commercially available laser systems.

## Introduction

In the last few years, laser-driven proton acceleration (LDPA) has become a growing field of research. The advent of high-power lasers (Dunne, 2006), which can produce accelerated bunches of particles (mainly protons and electrons), has attracted a strong interest in both the conventional and laser-plasma accelerator community. Compared to conventional accelerator machines, laser-driven particle accelerators have the advantage of potentially allowing more compact facilities due to the possibility of reaching accelerating fields in the order of TV/m, up to three orders of magnitude higher than what is typically obtained with radio frequency (RF)-based technology. In the case of LDPA, the target normal sheath acceleration (TNSA) is considered to be one of the most employed and reliable acceleration techniques (Wilks *et al.*, 1992). This scheme implements thin solid foils (with a thickness ranging from a few tens of nm up to a few tens of  $\mu$ m) that are irradiated with an ultra-intense ( $I > 10^{18}$  W/cm<sup>2</sup>), short laser pulse (i.e., with a duration from a fs to ps), allowing to accelerate proton beams to energies of up to tens of MeV (Macchi, 2017).

These laser-generated proton beams have unique characteristics, such as high charge ( $10^{13}$  particles/shot), high laminarity at the source, short bunch duration (ps at the source), and a high peak current (kA at the source). These characteristics make them desirable candidates for several applications that require one or more of the mentioned properties, such as biomedicine (tumor treatment, PET, radiography) (Bulanov *et al.*, 2002; Malka *et al.*, 2004), warm dense matter (Patel *et al.*, 2003; Antici *et al.*, 2006; Bulanov *et al.*, 2010; Mancic *et al.*, 2010), hybrid acceleration schemes (Antici *et al.*, 2008; Scisciò *et al.*, 2018) and material science (Dromey *et al.*, 2016; Barberio *et al.*, 2017a, 2018a, 2018b). Recently, the use of laser-accelerated proton beams as diagnostic for chemical analysis of cultural heritage (CH) artifacts has been investigated (Barberio *et al.*, 2017b; Barberio and Antici, 2019; Passoni *et al.*, 2019). The main challenge in this field is to collect as much information as possible regarding the chemical (Bertrand *et al.*, 2015; Santos *et al.*, 2016) and morphological (Schreiner *et al.*, 2007) state of the surface and the bulk of the samples (ceramics, paintings, bronze, etc.) while preventing any possible damage (Zucchiatti and Agulló-Lopez, 2012; Calligaro *et al.*, 2015; Lazic *et al.*, 2018) as well as find the best way for their conservation and restoration without any esthetical aspect modification. The particle-induced X-ray emission (PIXE) technique,

using protons as source, is performed in facilities such as the Accélérateur Grand Louvre d'analyse élémentaire (AGLAE) (Menu *et al.*, 1990; Radeponet *et al.*, 2018), located at the French Louvre laboratory – (C2RMF) (Zucchiatti and Redondo-Cubero, 2014), the AIFIRA facility at Centre d'Etudes Nucléaires Bordeaux-Gradignan (CENBG) (Barberet *et al.*, 2009; Sorieul *et al.*, 2014) and Istituto Nazionale di Fisica Nucleare–Laboratorio di tecniche nucleari per i Beni Culturali (INFN–LABEC) laboratory in Florence (Italy) (Giuntini *et al.*, 2007; Ezeh *et al.*, 2015; Re *et al.*, 2015). In these laboratories, conventional electrostatic accelerators (such as Van der Graff tandems or Pellatron types) (Mandò *et al.*, 2011) generate proton bunches with energies that range from 1 to 5 MeV, a beam current from few pA to nA (Chiari *et al.*, 2002), a beam charge of the order of nC (Pichon *et al.*, 2015). These proton beams irradiate the material samples (ceramics, paintings, bronze, etc.) and excite the emission of X-ray photons. The generated X-ray radiation can be measured with energy-dispersive devices (Bertrand *et al.*, 2015) and the retrieved energy spectrum provides information about the chemical components and their quantity present in the bulk of the analyzed samples.

The results reported in Barberio *et al.* (2017b) catalyzed the possibility of using a laser-driven proton source for PIXE spectroscopy as an alternative to conventional machines, implementing a “laser-driven PIXE”. Barberio *et al.* irradiated a silver sample with a laser-accelerated proton beam and were able to retrieve the chemical composition of the target with a single shot. They were able to demonstrate that the damage induced by the laser-accelerated protons was the same (if not lower) than what induced using conventional PIXE. That the short, but intense proton beam achievable using laser-driven PIXE could potentially have a positive impact on the damage induced on the artifact during the time of analysis is still under investigation.

Using a laser-driven proton source also has the advantage of an improved compactness of the acceleration section, compared to large conventional facilities such as NEW AGLAE ( $2 \times 30 \text{ m}^2$ ) (Pichon *et al.*, 2015) and INFN–LABEC ( $40 \times 15 \text{ m}^2$ ) (Grassi *et al.*, 2005). Using laser-PIXE, it is possible to scan larger volumes of the artworks with a single shot covering surfaces up to  $\text{cm}^2$ , while the final spot sizes that are typical of conventional accelerators go from a few  $\mu\text{m}$  ( $\sim 1\text{--}2 \mu\text{m}$ ) up to  $500 \mu\text{m}$ . The broad energy range of laser-driven proton sources permits the “tuning” of the beam energy in a broad range from few KeV to tens of MeV, potentially allowing a “layer by layer” analysis of the irradiated bulk material.

The total time for performing a full PIXE analysis depending on the allowable current on the sample and the required photons for having a reliable Signal-to-Noise ratio on the X-ray detector. Our technique is able to scan a larger surface and – depending on the energy spread – perform volumetric analysis, compared to conventional accelerators. In applications where this is useful, our technique can be quicker than conventional accelerators; however, when the useable current is limited, the energy spread needs to be low and the spot size is the same, the analysis time stays the same since this depends on the global flux.

Currently, the high beam divergence (few tens of degrees at the source) and the high energy spread (up to 100%) of laser-generated protons limit the efficiency of energy-selected beams for applications, including laser-PIXE. To overcome these issues, novel alternative acceleration techniques/regimes (Antici *et al.*, 2017; Macchi, 2017; Sharma, 2018) and the use of sophisticated targets (Barberio *et al.*, 2016; Sharma *et al.*, 2018) have been

studied theoretically and experimentally (Kraft *et al.*, 2018; Morrison *et al.*, 2018) with the aim of better controlling the acceleration mechanism and improving the proton beam yield.

Alternatively, to optimizing directly the laser-driven proton source, there have been different proposals manipulating the TNSA-generated proton beams downstream the laser–plasma interaction point using conventional accelerator devices, implementing so-called hybrid beamlines or post acceleration schemes. Numerous research groups have studied these schemes, in view of potential applications: using a RF cavity (Nakamura *et al.*, 2007), permanent quadrupoles magnets (PMQ) (Schollmeier *et al.*, 2008; Ter-Avetisyan *et al.*, 2008; Nishiuchi *et al.*, 2009) a compact travelling wave accelerator (Kar *et al.*, 2016), and adapting the beamlines to more specific applications, for example, the medical field (Busold *et al.*, 2013, 2014; Masood *et al.*, 2014; Romano *et al.*, 2016). In particular, between 2008 and 2011, several groups used a set of PQMs (Ter-Avetisyan *et al.*, 2008; Nishiuchi *et al.*, 2009), that, respectively, focused proton beams in the range of  $(3.7 \pm 0.3) \text{ MeV}$ , collected a final bunch of  $\sim 10^8$  particles and  $(2.4 \pm 0.1) \text{ MeV}$  with  $\sim 10^6$  particles. For reducing the energy spread of the protons, passive magnetic chicanes (Chen *et al.*, 2014; Scuderi *et al.*, 2014; Scisciò *et al.*, 2018) have been employed as energy selectors (ES).

In this work, we aim at optimizing the performance of a laser-driven hybrid beamline and compare it to typical parameters of conventional facilities dedicated to PIXE spectroscopy. The proposed beamline design includes an ES, with similar features as reported in Scisciò *et al.* (2018), followed by magnetic focusing devices [i.e., Permanent Magnet Quadrupoles (PQM)] in order to vary the final transverse dimensions of the energy-selected beam on the CH sample. The used ES provides the possibility of tuning the beam energy in the range that is typical for the PIXE analysis, that is, 1–5 MeV, reducing the initial energy spread to a final value of  $\leq 10\%$ . The ability to select different energies in a short time allows exploiting the possibility of performing a “layer by layer” analysis of the artifact (Barberio and Antici, 2019). The reduced energy spread also allows coupling the beam exiting the ES with focusing PQMs for modifying the analyzed surface on the CH sample (the broad energy spread of an unselected beam would lead to unsustainable chromatic effects in the focusing section). The variation of the PMQ's position between the ES and the sample allows tuning the final transverse beam spot size from a fraction of  $\text{mm}^2$  up to  $1\text{--}2 \text{ cm}^2$ . This potentially permits scanning a  $\text{cm}^2$  area with a few laser shots. We also estimate the final charge of the proton bunch, which needs to be high enough to be comparable to what is obtained on conventional facilities (in the order of nC/shot or a fraction of nC/shot if using a higher-repetition rate laser) (Pichon *et al.*, 2015). We study the main parameters of the transport line using beam dynamics simulation codes, namely TRACE3D and TSTEP, that are a standard tool for optimizing accelerator devices (Young, 1996; Crandall and Rusthoi, 1997).

The obtained results show that combining our compact hybrid beamline with a multi-Hz laser system allows to perform PIXE spectroscopy with features comparable to what obtained on conventional accelerators based on RF technology, potentially reducing the time of analysis of a larger surface to a few tens of seconds and the dimensions of the entire beamline (to a total length of  $< 1 \text{ m}$ ).

The paper is organized as follows: We initially describe the methodology for optimizing our proposed hybrid beamline scheme. In the section ‘Analysis of the ES’, we analyze only the

ES contribution and performance and we select the best features in terms of energy tunability and energy range. In the section ‘Optimization of the focusing section based on PMQs’, we present a study of the entire hybrid beamline including the focusing elements (i.e., the ES followed by one or two PMQs). We investigate three total length scenarios for our hybrid beamlines. These should fit in a medium/big size vacuum chamber. In LDPA, these have a typical diameter of around 1 m for TW laser systems (Fuchs *et al.*, 2005) or, in PW facilities, can reach a diameter of 2 m (Barberio *et al.*, 2017b). Our three scenarios are: (1) the ES coupled to one quadrupole aiming at a total length of 80 cm; (2) the ES coupled to one quadrupole aiming at a compact design of 50 cm total length; (3) the ES coupled to two PMQs in a FODO configuration. Finally, the conclusions are drawn.

### Analysis of the ES

The hybrid beamline that we have optimized for the PIXE analysis is qualitatively represented in Figure 1 and has been studied using the above-mentioned codes TRACE3D and TSTEP.

At first, we have studied the ES that accounts for reducing the energy spread of the proton bunch. We have adopted a similar methodology as reported in Scisciò *et al.* (2018).

Commonly, an ES is implemented as follows: a magnetic dipole chicane with one entrance slit and one selecting slit (see Fig. 1) (Chen *et al.*, 2014; Scuderi *et al.*, 2014; Scisciò *et al.*, 2018). The entrance slit ( $a_1$ ) reduces the initial divergence of the beam that enters the dipoles. The particles (accelerated along  $z$ ) are then dispersed transversely along  $x$  by a distance that depends on their velocity. The aperture of the second slit ( $a_2$ ), which is movable on the dispersion plane along the  $x$ -axis, accounts for the energy selection of the protons. After the central selecting slit ( $a_2$ ) – see Figure 1 – two additional dipoles realign the selected beam along the initial propagation axis. We limit our beamline design to using only two dipoles. Adding further two dipoles would allow bending the beam back to its original trajectory axis. However, the characteristics of the beam using 4 dipoles are not as competitive as using only 2 dipoles. For the applications, it is not relevant to keep the beam on its original propagation axis. We therefore limit the present study to only 2 dipoles.

The main dipole parameters, as reported in Figure 1, are a length of  $l_d = 10$  cm, a width of  $w_d = 10$  cm, a vertical gap of  $g = 0.9$  cm (i.e., the dipole gap in  $y$ -direction), and magnetic field  $B_y = 0.92$  T (incoming magnetic field for the first dipole and outgoing magnetic field for the second one). These parameters are similar to what is reported in Scisciò *et al.* (2018), where a selector in the energy range 2–20 MeV has been optimized and has been adapted to our range of 1–5 MeV. For studying the energy selection process, we simulate an initial proton beam having a uniform energy distribution with energy spread  $\Delta E/E_0$  of 100% (the black spectrum of Fig. 2) and evaluate the final energy spread after the selection slit (the colored spectra of Fig. 2). The first selector parameter that we analyze is the initial beam divergence: we aim at indicating a maximum initial divergence that is compatible with the final beam parameters that are required for the PIXE analysis (Grassi *et al.*, 2005; Pichon *et al.*, 2015).

The initial divergence is determined by the aperture  $a_1$  of the first slit and its distance  $d$  from the laser–plasma source. For example, an aperture  $a_1 = 500$   $\mu\text{m}$  and an initial divergence of 3 mrad correspond to a distance between the laser proton source and the entrance of the ES of  $d = 8$  cm. We vary the initial

divergence from a minimum of 3 mrad up to 10 mrad (half angle) for the three energy cases 1, 3, and 5 MeV. The final achieved energy spread is reported in Figure 2, where it is shown that the increase in the initial divergence leads to an increase in the final energy spread. The simulations show that this increase starts to be particularly significant for a divergence  $\geq 7$  mrad for the cases of 3 and 5 MeV. When selecting 1 MeV protons (Fig. 2a), the FWHM energy spread ranges from 3% (for 3 mrad initial divergence) to 11% (10 mrad initial divergence). For the cases of 3 and 5 MeV (Fig. 2b and 2c), an initial divergence of 10 mrad leads to a final energy spread of 23 and 30%, respectively. This is an increase of a factor three with respect to the case of an initial divergence of 3 mrad (8 and 10% final energy spread, for 3 and 5 MeV, respectively).

This is due, as reported in Chen *et al.* (2014) and Scisciò *et al.* (2018), to the natural intrinsic divergence and emittance growth of the proton beam at the source (Migliorati *et al.*, 2013) which adds further deviation from the normal trajectory induced by the magnetic field of the dipoles.

According to these results, we define our optimal initial divergence as a compromise between the final energy spread, which should be  $\leq 10\%$ , and the number of particles transmitted through the slit, which obviously decrease in case of smaller apertures. Moreover, this energy spread range is acceptable, considering that the energy interval 1–5 MeV allows to investigate the first few  $\mu\text{m}$  of CH samples. For the initial slit at a distance  $d = 8$  cm from the laser–plasma source in the case of 1 MeV, we use an aperture of  $a_1 = 800$   $\mu\text{m}$ , obtaining a divergence of 5 mrad. Similarly, for both 3 and 5 MeV cases, we choose an aperture of  $a_1 = 500$   $\mu\text{m}$  leading to an initial divergence of 3 mrad.

We also analyze the aperture  $a_2$  of the selecting slit that is needed for the final energy selection and allows obtaining the narrow energy spread. The width of the aperture should be a compromise between the desired final energy spread and the number of transmitted particles that is required in order to have a final charge that is comparable to what is implemented on conventional PIXE facilities. A smaller value of  $a_2$  leads to a reduction of the final number of particles that is transmitted through the selector. For selecting lower energy particles, which experience a larger displacement by the dipole field, a larger aperture is allowed in order to obtain a final energy spread  $\leq 10\%$ . Therefore, we choose as a compromise an aperture of the central slit of  $a_2 = 1000$   $\mu\text{m}$  for selecting a 1 MeV beam and an aperture of  $a_2 = 500$   $\mu\text{m}$  for the cases of 3 and 5 MeV. These three choices of different energies are the most employed energies when using PIXE applications (Grassi *et al.*, 2005) and allow obtaining a FWHM final energy spread  $\leq 10\%$  in the energy range of our interest. In Figure 2d, we report the final energy spectra of 1, 3, and 5 MeV beams, selected using these optimized parameters of initial divergence, that are, the distance  $d$ , slit width  $a_1$  and slit width  $a_2$ .

For a selected central energy (1–3–5 MeV), we obtain the respective selected final energy range (Fig. 2d). We define the transmission efficiency of the beamline  $\eta_{\text{BL}}$  as the ratio between the number of particles that reach the CH sample (final beam) and the number of particles that pass through the initial slit of the ES, in the same final selected energy range. For the central energy 1 MeV, we obtain the value  $\eta_{\text{BL}} \simeq 12\%$ , while for the central energies 3 and 5 MeV, the value of  $\eta_{\text{BL}}$  is  $\simeq 9\%$ . With  $\eta_{\text{BL}}$ , we do not take into account the losses induced by the collimation slit (with width  $a_1$ ). These initial losses strongly depend on the characteristics of the laser–plasma interaction that

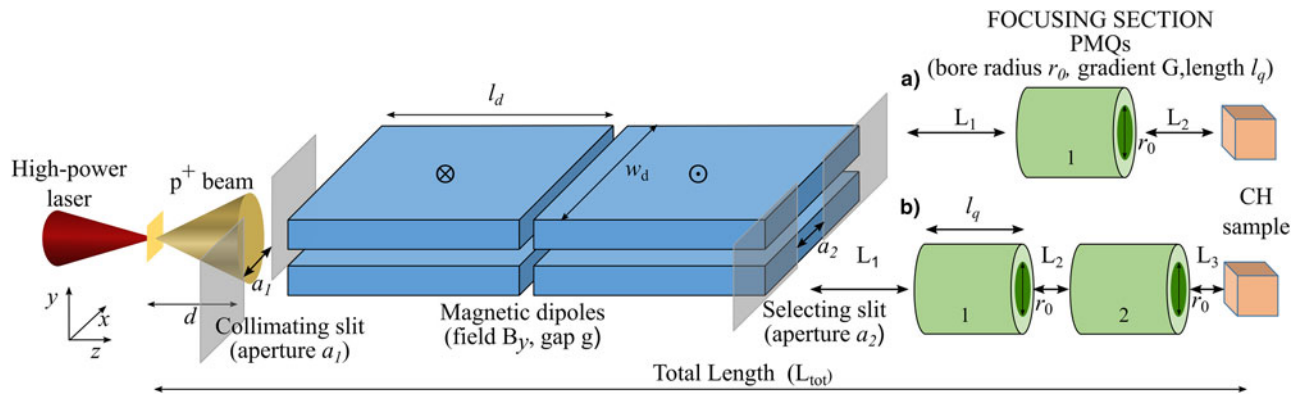


**Fig. 1.** Qualitative scheme of the hybrid beamline. It is composed of an ES, consisting of two dipoles [both of length  $l_d = 10$  cm; width  $w_d = 10$  cm;  $B_y = 0.92$  T (incoming magnetic field for the first dipole and outgoing magnetic field for the second one), gap size of 0.9 cm], a collimating slit ( $a_1$ ) and the central selecting slit ( $a_2$ ), followed by one or multiple PMQs. The first slit, with distance from the source  $d$  and aperture  $a_1$  can be varied for collimating the beam, i.e. reducing the initial divergence. The particles are then displaced transversely (along the  $x$ -axis) with respect to the direction of propagation ( $z$ ) by the bending dipoles according to their velocity. The aperture  $a_2$  of the selecting slit provides the energy selection and reduces the final energy spread of the protons. The PMQ parameters [with length  $l_q$ , bore radius  $r_0$  (internal diameter) and the gradient  $G$ ] are optimized in order to focus/defocus the final transverse spot size on the irradiated sample. We consider as possible focusing sections two scenarios: ES followed by one PMQ (a) and ES followed by two PMQs (b). The total distance  $L_{\text{tot}}$  is maximum 80 cm and the drifts are, respectively,  $L_1$  and  $L_2$  in the case (a) and  $L_1, L_2, L_3$  in case (b). By varying the values of distances  $L_1, L_2$  or  $L_1, L_2, L_3$ , the transverse dimensions of the final beam can be tuned.

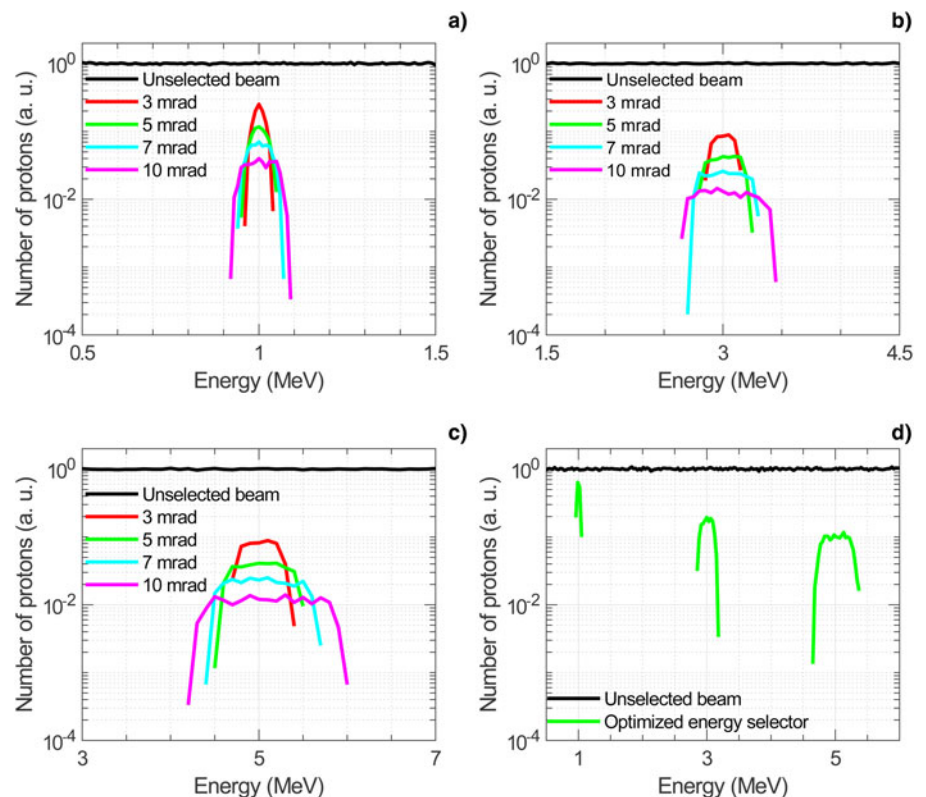


**Fig. 2.** Final energy spread as function of the initial divergence, for the case of 1 MeV (a), 3 MeV (b), and 5 MeV (c), at the exit of the selector. The initial divergence has the values: 3 mrad (red color), 5 mrad (green color), 7 mrad (light blue color), 10 mrad (magenta color). The dark black curve represents the unselected beam at the entrance of the selector. (d) Final energy spectra in the case of 1, 3, and 5 MeV beams, selected using 5 mrad and  $a_2 = 1000 \mu\text{m}$  (1 MeV beam), and 3 mrad and  $a_2 = 500 \mu\text{m}$  (3 and 5 MeV beams).

generates the protons, such as the beam energy-divergence distribution at the source. Since we do not focus our study on a specific case of laser-plasma interaction conditions, we estimate these losses with  $\eta_s$  from the solid angle of the collimation slit's aperture. The horizontal divergence at the source is reduced by the initial collimating slit to a value of 3 mrad (for the cases of 3 and 5 MeV, 5 mrad for the case of 1 MeV). In the vertical plane, the divergence is only limited by the vertical aperture of the dipoles ( $\sim 1$  cm), corresponding to a half angle of 56 mrad.

Taking into account that the mean divergence of a TNSA beam at the source typically is about  $15^\circ$  half angle (Mancic *et al.*, 2010; Green *et al.*, 2014), corresponding to a solid angle of around 0.21 steradian, the collimation slit induces a loss of  $\eta_s = 0.31\%$  for the energy cases of 3 and 5 MeV. This value is higher for the case of 1 MeV protons where we obtain  $\eta_s = 0.50\%$ , due to the initial horizontal collimation of 5 mrad that is achieved with a wider slit aperture ( $a_1 = 800 \mu\text{m}$ ). The final total transport efficiency (i.e., from the source to the end of the line) is  $\eta_T = \eta_s \cdot$

$\eta_{BL}$  and we obtain  $\eta_T = 0.059\%$  for the 1 MeV beam and  $\eta_T = 0.028\%$  and for the 3 and 5 MeV beams. This efficiency could be improved using a focusing section before entering the first dipole.

With these values, it is possible to estimate the bunch charge that is delivered to the sample for each mean energy within one single laser shot. From a typical TNSA proton spectrum (Fuchs *et al.*, 2005; Fourmaux *et al.*, 2013; Green *et al.*, 2014), obtained using a TW-class laser system with a repetition rate in the range 1–10 Hz, we can set values for the initial charge at the source. Taking as benchmark for the number of particles, a typical proton spectrum as produced by a high-power short-pulse laser of new generation (Green *et al.*, 2014), and considering the central energies of 1, 3, and 5 MeV with a final energy spread of, respectively, 6, 8, and 10% we obtain about  $5 \cdot 10^{11}$ ,  $5 \cdot 10^{11}$ , and  $1 \cdot 10^{11}$  particles per shot, respectively. After all the losses along the line, the final charge on the sample is  $\sim 0.05$  nC/shot for 1 MeV,  $\sim 0.02$  nC/shot for 3 MeV, and  $\sim 0.004$  nC/shot for 5 MeV. A reference value for the total charge that is used in order to retrieve the PIXE signal from a scanned area of the sample is reported in Pichon *et al.* (2015) where 1.8 nC are used to scan a sub-millimetric area. Coupling our beamline to a 1 Hz high-intense laser system allows cumulating a similar final charge in less than 10 min irradiation for the 1–3–5 MeV beams. These time expositions can be further decreased by a factor 10 using the new upcoming 10 Hz high-intensity laser systems (Kühn *et al.*, 2017; Mondal *et al.*, 2018; Roso, 2018).

### Optimization of the focusing section based on PMQs

This section describes the results obtained from the second set of simulations that are performed in order to investigate the combination of the ES with the focusing/defocusing PMQs. For optimizing our design, we consider two different scenarios. At first, we aim at focusing/defocusing the proton beam using a single quadrupole and for the total length of the beamline (Fig. 1) we consider a case with 50 cm total length (this represents a compact beamline that can be easily adapted to a medium/large vacuum chamber (Fuchs *et al.*, 2005; Barberio *et al.*, 2017b; Nilsson *et al.*, 2019; Vallières *et al.*, 2019) and a case with 80 cm total length [an extended version where the range of the final spot size of the beam is broader but presumably requires an extension if implemented in a chamber of common dimensions, which can also be desirable for inserting additional diagnostics (Bolton *et al.*, 2014)]. Secondly, we study the case where two quadrupoles are used, in a FODO configuration, in order to focus/defocus the beam. In that case, the total length of the beamline is about 80 cm. The distance between the source and the sample has a fixed value for each scenario that we study: in this way, we manipulate the proton beam (i.e., change the selected energy or vary the final spot size) without the necessity of displacing the sample.

The key design parameters of the PQMs are the bore radius  $r_0$ , the magnetic field gradient  $G$ , and the magnetic length  $l_q$ . The maximum achievable gradient is related to the magnetic field  $B_0$  on the quadrupole's pole tip and the bore radius, as  $G = B_0/r_0$ . We choose for our beamline design a PMQ length of  $l_q = 4.5$  cm and a bore radius of  $r_0 = 1$  cm. These parameters can be easily obtained with the existing permanent magnet technology (Halbach and Holsinger, 1976; Eichner *et al.*, 2007; Nirikko *et al.*, 2013; Marteau *et al.*, 2017) and allow us to keep the dimensions of the beamline compact. Using rare-earth materials, these features allow obtaining a value of  $B_0$  in the range of hundreds

of mT (Eichner *et al.*, 2007; Nirikko *et al.*, 2013) and a field gradient in the order of several tens of T/m.

### Focusing section based on a single quadrupole

We first perform TRACE3D simulations, which evaluate the beam envelope along the line, in order to optimize the focusing section. The obtained results are then compared and validated with TSTEP simulations, performed in the same conditions (i.e., same PMQ parameters, same distances between the transport elements). TRACE3D provides an optimization routine that indicates the optimal parameters of the line based on matching conditions of the beam Twiss parameters ( $\alpha$ ,  $\beta$ ,  $\gamma$ ) between two different positions of the transport line (in our case between the exit of the ES and the irradiated sample). The aim is to optimize the position of the quadrupole for obtaining a variable final beam transverse dimension on the sample, ranging from a few mm up to the order of cm.

For the three mean energies of our interest 1, 3, and 5 MeV, the simulated gradient of the quadrupoles is set at  $G = 60$  T/m (with magnetic length  $l_q = 4.5$  cm). This value is obtained from preliminary optimizations with TRACE3D where different gradients have been exploited: it is a good compromise for operating at these different energies and it is a compatible value with the typical field intensities of commercial PMQs of this size. The initial values of the Twiss parameters ( $\alpha$ ,  $\beta$ ,  $\gamma$ ) are calculated according to the transverse beam geometry at the exit of the ES and represent the initial beam conditions for the TRACE3D simulations. The horizontal (in  $x$ -direction) dimension of the beam is determined by the aperture  $a_2$  of the selecting slit of the ES [1 mm for 1 MeV, 500  $\mu$ m for 3 (Fig. 3a) and 5 MeV], while the vertical dimension (along  $y$ ) depends by the dipoles' s gap  $G$  (the vertical aperture is of 0.9 cm). These parameters are reported in Figure 3b where the phase space of the protons at the end of the ES is plotted for the case of 3 MeV beam energy.

For calculating the optimal position of the PMQ between the selector and the sample, we set the drift spaces before and after the quadrupole location, indicated in Figure 3a with  $L_1$  and  $L_2$ , as free parameters. We define conditions on the final Twiss parameters on the  $y$ -coordinate with the values  $\alpha_y = 0$  and  $\beta_y = 0.008$  m for obtaining a collimated beam and a decreased final spot size (small irradiated area on the sample). Then we repeat the optimization routine with the values  $\alpha_y = 28$  and  $\beta_y = 1.4804$  m for obtaining a defocused beam, that is, a final spot size with increased dimensions (large irradiated area on the sample). The numerical values of  $\alpha_y$ ,  $\beta_y$  reported and respectively associated with the smallest and largest irradiated areas on the sample, are calculated, through Matlab routines, from TSTEP data simulations and are fixed and used as references for the optimization runs. The total distance between the source and the final longitudinal position (i.e., the position where the irradiated sample is placed) is fixed at 80 cm. The matching routine retrieves, for both, the smallest and the largest spot size, the optimized values of  $L_1$  and  $L_2$ . In Figure 3c and 3d, we report, as an example among the three possible energy cases, the final transverse phase space obtained with the TRACE3D optimization routine and refined with a particle tracking simulation with TSTEP, of a beam with a mean energy of 3 MeV passing through a  $y$ -focusing PMQ that has the following optimized distances:  $L_1 = 25.7$  cm,  $L_2 = 9.8$  cm for the focused, small final spot size and  $L_1 = 3$  cm,  $L_2 = 32.5$  cm for the defocused, large final spot size.

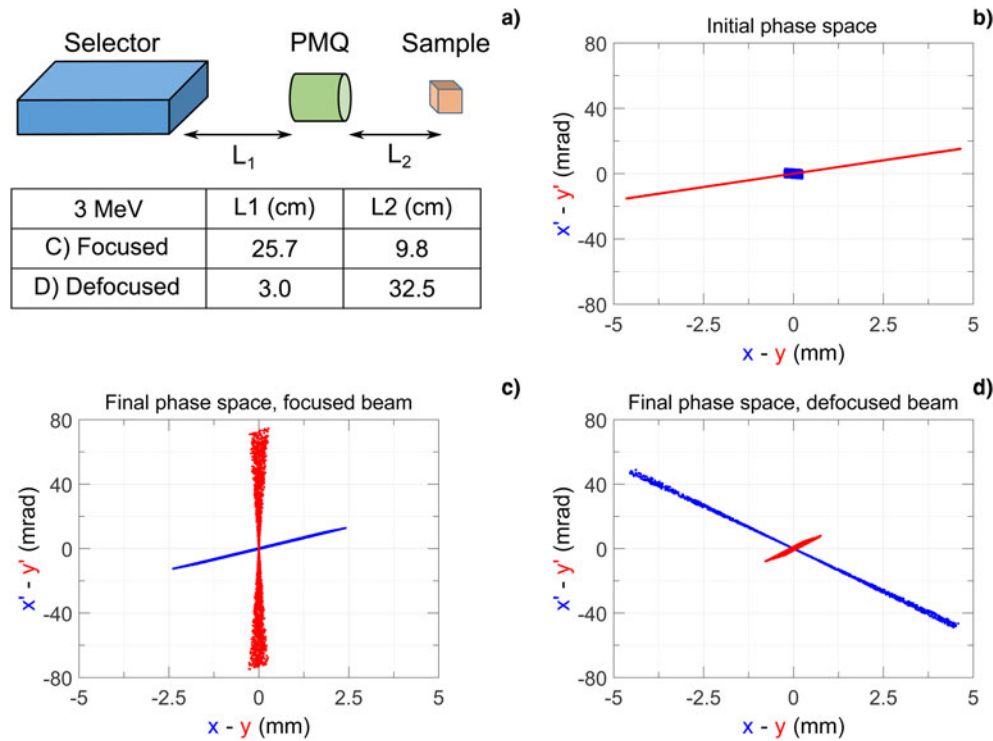


**Fig. 3.** (a) Scheme of the simulated beamline. The numbers in the table indicate the values of  $L_1$  and  $L_2$  for the corresponding colored plot in (c) and (d). (b) Initial phase space, as obtained at the exit of the selector that is used for calculating the input Twiss parameters of the TRACE3D simulations. (c) and (d) Final phase space obtained with the TRACE3D optimized distances  $L_1$  and  $L_2$  for a focused and defocused beam, respectively.

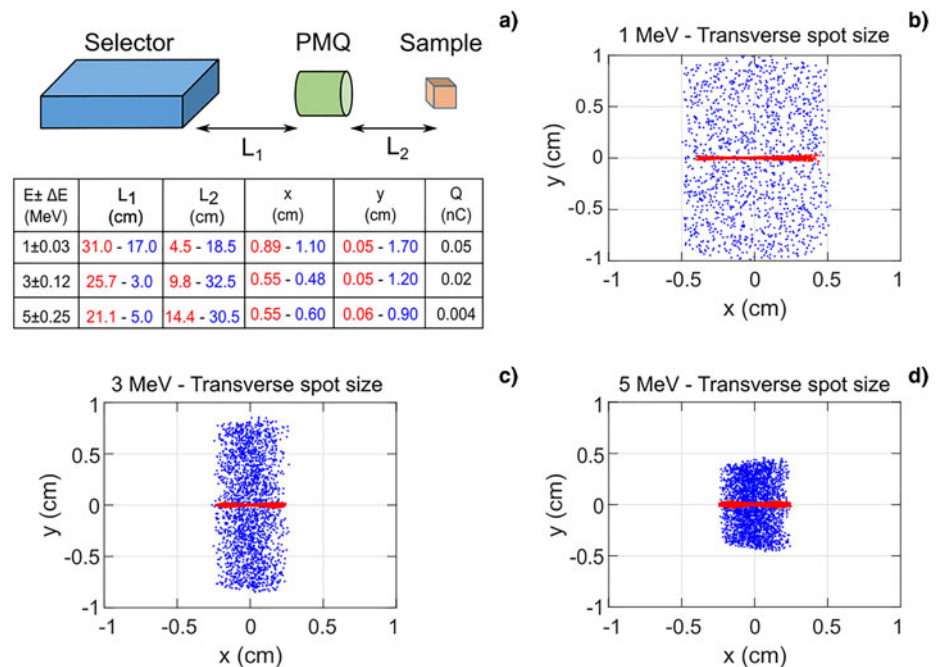


**Fig. 4.** (a) Scheme of the simulated beamline and position of the PMQ, charge, energy, and final transverse spot size dimensions for the analyzed cases. (b)–(d) Final transverse dimensions of the focused (red plot) and defocused (blue plot) proton beam for the cases of 1, 3, and 5 MeV, respectively. These spot sizes are obtained with a single PMQ after the selector, having a length of 4.5 cm and a magnetic field gradient of 60 T/m. The entire beamline (from the proton source to the CH sample) has a length of 80 cm.

These optimized parameters of the beamline are simulated again with the particle tracking code TSTEP that computes the final transverse spot of the beam from a realistic proton distribution, tracking the trajectory of the single macroparticles. We repeat the process for the energies 1, 3, and 5 MeV: the results are shown in Figure 4. The final energy spread is not altered

by the addition of one (or multiple, as discussed later) PMQ: the results of Figure 2 remain unchanged. The value of  $\eta_{BL}$  does not change when adding these newly optimized PMQs: no additional particle losses are induced and the overall transport efficiencies are the same as calculated in the previous section. From the plots of Figure 4a, one can see that with this

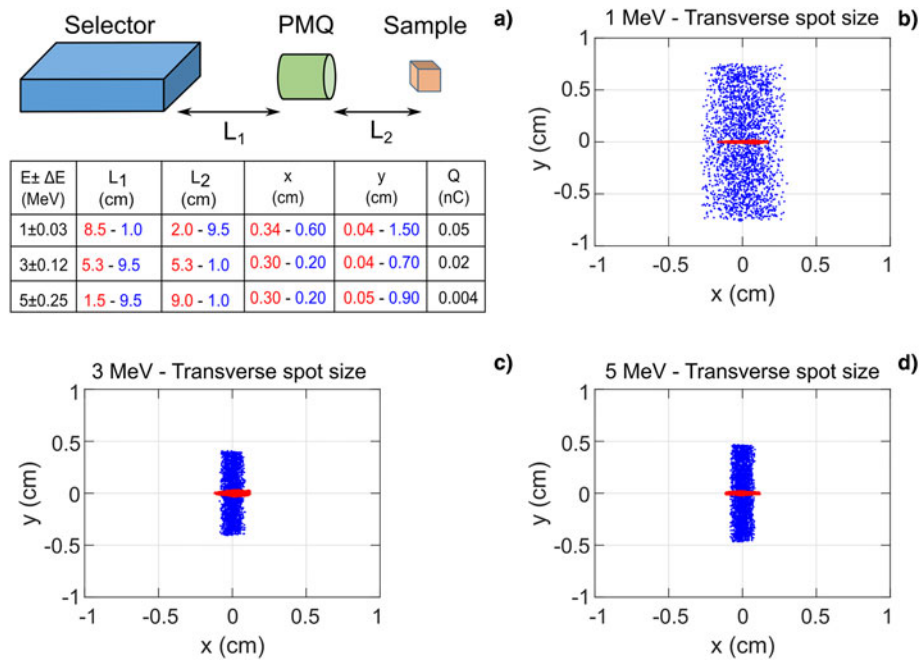


**Fig. 5.** (a) Scheme of the simulated beamline and position of the PMQ, charge, energy, and final transverse spot size dimensions for the analyzed cases. (b)–(d) Final transverse dimensions of the focused (red plot) and defocused (blue plot) proton beam for the cases of 1, 3, and 5 MeV, respectively. These spot sizes are obtained with a single PMQ after the selector, having a length of 4.5 cm and a magnetic field gradient of 100 T/m. The entire beamline (from the proton source to the CH sample) has a length of 50 cm.

configuration it is possible to scan areas of the CH sample with dimensions in the  $\text{cm}^2$  range, represented in Figure 4b–d with the blue dots. Simply by changing the position of the PMQ and keeping all other parameters unvaried, it is possible to focus the beam (red plot) and achieve a precision on the vertical axis of  $<1$  mm.

As an alternative to the 80 cm long beamline, we also study the possibility of reducing the total length in order to design a line that can possibly fit in a medium size experimental chamber. We aim at obtaining a variable final spot size in the same range as for the longer beamline case (from the mm to the cm range) within a total distance of about 50 cm from the laser–plasma source. We repeat the same procedure as before: the TRACE3D matching algorithm provides indications for the optimized position (for small/large final spot size) and gradient of the PMQ. These values are then validated by additional TSTEP simulations. The optimized design for the case of a 50 cm long beamline is reported in Figure 5a, where the layout is shown and the final beam spot sizes for the energy cases 1–3–5 MeV are plotted. In Figure 5b–d, the smallest achievable spot size as identified by the red dots and the largest achievable spot size (blue dots) are shown.

As before, the used PMQ has a length of  $l_q = 4.5$  cm and a bore radius  $r_0 = 1$  cm. The gradient needs to be increased to  $G = 100$  T/m. This allows to shorten the focal distance and obtain both the biggest and the smallest final transverse spot sizes on the CH sample. As shown in Figure 5b–d, this beamline allows to enlarge the final vertical ( $y$ -axis) transverse dimension up to about 1 cm for all the analyzed energies. Final spot sizes in the sub-millimetric range are also obtainable for all mean energies by varying the position of the PMQ between the exit of the ES and the end of transport line. In the 3 MeV case, by placing the PMQ 5.3 cm after the exit of the selector, a final vertical dimension of  $\sim 0.4$  mm is obtained (see Fig. 5c). With this compact scheme, the final energy spread is the same as what is reported in Figure 2 and the transport efficiency is not influenced by the focusing section: as before, we have  $\eta_T = 0.028\%$  (3 and 5 MeV) and  $\eta_T = 0.059\%$  (1 MeV).

### ES followed by two PQMs

As an alternative to a focusing section with only one PMQ, we also study the possibility of implementing two PQMs after the ES. We use the same methodology as for the beamlines analyzed before. In the three energy cases reported in Figure 6, the two PQMs are in a FODO configuration where the first quadrupole (closer to the selector) focuses in  $y$  and the second focuses in  $x$ . We firstly perform a series of preliminary TRACE3D simulations in order to find a viable gradient compromise for all three energy cases: the optimized parameters of the previous configuration, that are  $l_q = 4.5$  cm,  $G = 60$  T/m, and  $r_0 = 1$  cm for both PQMs, are suitable for the FODO scheme. The additional PMQ, if carefully optimized, allows to obtain more symmetric spot sizes (in  $x$  and  $y$ ) compared to the previous cases with a single PMQ where asymmetric, elongated final spots are obtained.

After having optimized the PMQ gradients, we have performed additional TRACE3D simulations in order to optimize their position with respect to the exit of the ES: similarly, as before, our goal is to obtain an optimized spacing of the PMQs for a focused (small) and defocused (large) spot size on the irradiated sample, by keeping a fixed distance between the proton source and the sample. The optimization regarding the gradients and the positions of the PMQ pairs, provided by TRACE3D simulations, are compared and tested with TSTEP: the particle tracking results allow a further tuning of the spacing and we achieve the final spot sizes for the different energy cases reported in Figure 6. These optimized results allow us to find small/large quasi-symmetric transverse spot sizes with the spacing details that are showed in Figure 6a. The number of transmitted particles keeps unaltered by the addition of one PMQ. The final transverse spot sizes are in the  $\text{cm}^2$  range when the PMQ spacing is optimized for obtaining a defocused beam (see Fig. 6b–d) where a final spot size of  $>1 \text{ cm}^2$  is obtained for the 1 MeV case and about  $0.6 \times 0.6$  cm for the 5 MeV case. When the spacing is optimized for focusing the beam on the sample, small spot sizes are obtained: we obtain millimetric dimensions on both transverse axes, for all investigated energies (the smallest

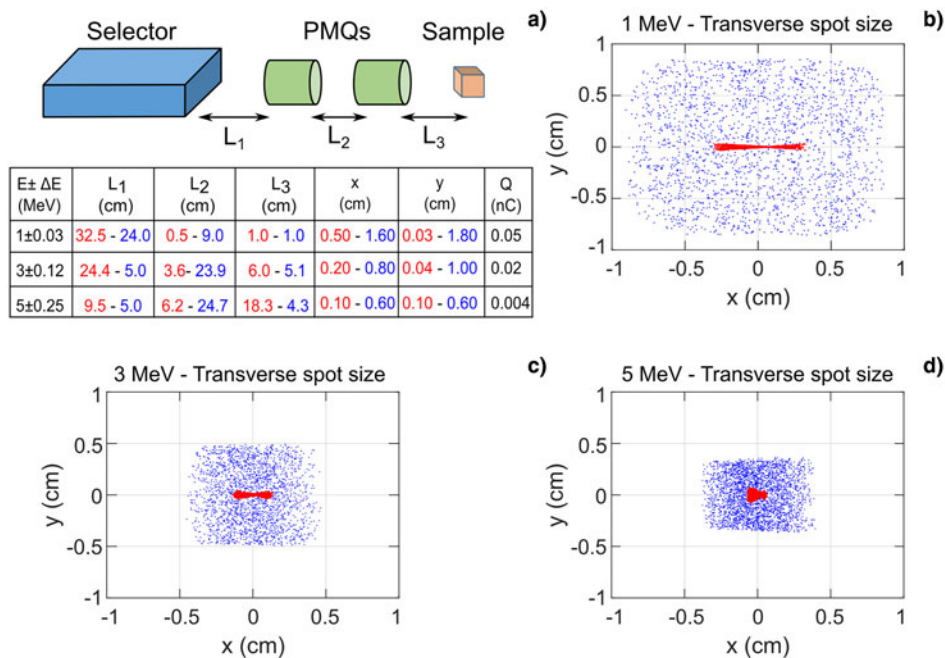


**Fig. 6.** (a) Scheme of the simulated beamline and position of the PMQ, charge, energy, and final transverse spot size dimensions for the analyzed cases. (b)–(d) Final transverse dimensions of the focused (red plot) and defocused (blue plot) proton beam for the cases of 1, 3, and 5 MeV, respectively. These spot sizes are obtained with a pair of PMQs in a FODO configuration. They have a length of 4.5 cm and a magnetic field gradient of 60 T/m. The first PMQ focuses in  $y$ -direction, the second PMQ focuses in  $x$ -direction. The entire beamline (from the proton source to the CH sample) has a length of  $\sim 80$  cm.

spot is achieved for the 5 MeV case with  $\sim 1$  mm on both transverse axis). In this case with a PMQ section implementing a quadrupole pair, the total length of the beamline is of  $\sim 80$  cm for all energies, that is, the same order of magnitude as the cases with a single PMQ. This allows to fix the position of the irradiated sample with respect to the proton source and the variation of the spot size dimension and energy can be achieved by changing the spacing of the PMQs after the selector. Compared to the scheme with a single PMQ, this beamline has the advantage of producing quasi-symmetric final spot sizes. This can potentially be an advantage for scanning small areas (below 1 mm) on the sample with a more concentrated charge and an improved precision.

We can perform “layer-by-layer” PIXE analysis without resetting the electrostatic accelerator as it is done conventionally (Chiari *et al.*, 2002; Grassi *et al.*, 2005). The overall (i.e., from the proton source to the sample) transmission efficiency is  $\eta_T = 0.028\%$  for the 3 and 5 MeV beams, while for the case of 1 MeV we obtain  $\eta_T = 0.059\%$ . With these values, after taking into account all the losses along the line, it is possible to deliver a final charge on the sample of  $\sim 0.05$  nC/shot for 1 MeV,  $\sim 0.02$  nC/shot for 3 MeV, and  $\sim 0.004$  nC/shot for 5 MeV (section ‘Analysis of the ES’). As benchmark for comparing these values to convention PIXE, we consider a total charge of 1.8 nC used to scan a sub-millimetric area (Pichon *et al.*, 2015). The coupling of our beamline with a 1 Hz high-intense laser system allows cumulating a similar final charge in less than 10 min irradiation for all the three energy cases (1–3–5 MeV beams). The use of the new upcoming 10 Hz high-intensity laser systems (Kühn *et al.*, 2017; Mondal *et al.*, 2018; Roso, 2018) will allow to further decrease these time expositions by a factor 10.

Especially for scanning a large surface of the sample, the laser-driven PIXE represents a valid alternative to the conventional technique, which requires a pencil scan that lasts several minutes.

## Conclusions

The present here a compact beamline based on laser-accelerated protons coupled to an ES and focusing quadrupoles, for

application of laser-PIXE. Our design allows obtaining a feasible and versatile scheme, yielding to a final beam with variable transverse dimensions and a reduced energy spread. The simulated structure is compact (the largest version of it is less than 1 m long) and allows selecting proton beams with mean energies in the range 1–5 MeV achieving final FWHM energy spread of  $\sim 10\%$ . The implementation of the PMQs after the selector provides a broad range of final transverse dimensions, with negligible modification to the transport efficiency and final energy spread. With a single PMQ, we achieve a final vertical dimension of the beam ranging from the cm scale to  $< 1$  mm. Using a PMQ pair, we obtain more symmetric spot sizes in the same range. The overall (i.e., from the proton source to the sample) transmission efficiency is  $\eta_T = 0.028\%$  for the 3 and 5 MeV beams, while for the case of 1 MeV, we obtain  $\eta_T = 0.059\%$ . With these values, after taking into account all the losses along the line, it is possible to deliver a final charge on the sample of  $\sim 0.05$  nC/shot for 1 MeV,  $\sim 0.02$  nC/shot for 3 MeV, and  $\sim 0.004$  nC/shot for 5 MeV (section ‘Analysis of the ES’). Our results provide helpful guidelines and a consistent methodology for designing and optimizing a beamline for laser-accelerated protons in order to exploit ion beam analysis for CH.

**Acknowledgements.** We thank Marianna Barberio for the precious support and useful discussions. This work is supported by the European Regional Development Fund (GINOP-2.3.6-15-2015-00001). Patrizio Antici acknowledges the support by NSERC Discovery Grant (RGPIN-2018-05772), ComputeCanada (Job: pve-323-ac, P. Antici).

## References

- Antici P, Fuchs J, Atzeni S, Benuzzi A, Brambrink E, Esposito M, Koenig M, Rasio A, Schreiber J, Schiavi A and Audebert P (2006) Isochoric heating of matter by laser-accelerated high-energy protons. *Journal de Physique IV (Proceedings)* **133**, 1077–1079.
- Antici P, Fazi M, Lombardi A, Migliorati M, Palumbo L, Audebert P and Fuchs J (2008) Numerical study of a linear accelerator using laser-generated proton beams as a source. *Journal of Applied Physics* **104**, 124901.
- Antici P, Boella E, Chen SN, Andrews DS, Barberio M, Böker J, Cardelli F, Feugas JL, Glessner M, Nicolai P, Romagnani L, Scisciò M,



- Starodubtsev M, Willi O, Kieffer JC, Tikhonchuk V, Pépin H, Silva LO, d' Humières E and Fuchs J (2017) Acceleration of collimated 45 MeV protons by collisionless shocks driven in low-density, large-scale gradient plasmas by a 1020 W/cm<sup>2</sup>, 1 μm laser. *Scientific Reports* 7, 16463.
- Barberet P, Incerti S, Andersson F, Delalée F, Serani L and Moretto P (2009) Technical description of the CENBG nanobeam line. *Nuclear Instruments and Methods in Physics Research Section B: Beam Interactions with Materials and Atoms* 267, 2003–2007.
- Barberio M and Antici P (2019) Laser-PIXE using laser-accelerated proton beams. *Scientific Reports* 9, 6855.
- Barberio M, Scisciò M, Veltri S and Antici P (2016) Fabrication of nanostructured targets for improved laser-driven proton acceleration. *Superlattices and Microstructures* 95, 159–163.
- Barberio M, Scisciò M, Vallières S, Veltri S, Morabito A and Antici P (2017a) Laser-generated proton beams for high-precision ultra-fast crystal synthesis. *Scientific Reports* 7, 12522.
- Barberio M, Veltri S, Scisciò M and Antici P (2017b) Laser-accelerated proton beams as diagnostics for cultural heritage. *Scientific Reports* 7, 40415.
- Barberio M, Scisciò M, Vallières S, Cardelli F, Chen SN, Famulari G, Gangolf T, Revet G, Schiavi A, Senzacqua M and Antici P (2018a) Laser-accelerated particle beams for stress testing of materials. *Nature Communications* 9, 372.
- Barberio M, Vallières S, Scisciò M, Kolhatkar G, Ruediger A and Antici P (2018b) Graphitization of diamond by laser-accelerated proton beams. *Carbon* 139, 531–537.
- Bertrand L, Schöeder S, Anglos D, Breese MBH, Janssens K, Moini M and Simon A (2015) Mitigation strategies for radiation damage in the analysis of ancient materials. *TrAC – Trends in Analytical Chemistry* 66, 128–145.
- Bolton PR, Borghesi M, Brenner C, Carroll DC, De Martinis C, Fiorini F, Flacco A, Floquet V, Fuchs J, Gallegos P, Giove D, Green JS, Green S, Jones B, Kirby D, McKenna P, Neely D, Nuesslin F, Prasad R, Reinhard S, Roth M, Schramm U, Scott GG, Ter-Avetisyan S, Tolley M, Turchettin G and Wilkens JJ (2014) Instrumentation for diagnostics and control of laser-accelerated proton (ion) beams. *Physica Medica* 30, 255–270.
- Bulanov S, Esirkepov TZ, Khoroshkov V, Kuznetsov A and Pegoraro F (2002) Oncological hadrontherapy with laser ion accelerators. *Physics Letters A* 299, 240–247.
- Bulanov SS, Bychenkov VY, Chvykov V, Kalinchenko G, Litzenberg DW, Matsuoka T, Thomas AGR, Willingale L, Yanovsky V, Krushelnick K and Maksimchuk A (2010) Generation of GeV protons from 1 PW laser interaction with near critical density targets. *Physics of Plasmas* 17, 043105.
- Busold S, Schumacher D, Deppert O, Brabetz C, Frydrych S, Kroll F, Joost M, Al-Omari H, Blažević A, Zielbauer B, Hofmann I, Bagnoud V, Cowan TE and Roth M (2013) Focusing and transport of high-intensity multi-MeV proton bunches from a compact laser-driven source. *Physical Review Special Topics – Accelerators and Beams* 16, 101302.
- Busold S, Schumacher D, Deppert O, Brabetz C, Kroll F, Blažević A, Bagnoud V and Roth M (2014) Commissioning of a compact laser-based proton beam line for high intensity bunches around 10 MeV. *Physical Review Special Topics – Accelerators and Beams* 17, 031302.
- Calligaro T, Gonzalez V and Pichon L (2015) PIXE analysis of historical paintings: is the gain worth the risk? *Nuclear Instruments and Methods in Physics Research, Section B: Beam Interactions with Materials and Atoms* 363, 135–143.
- Chen SN, Gauthier M, Higginson DP, Dorard S, Mangia F, Riquier R, Atzeni S, Marquès J-R and Fuchs J (2014) Monochromatic short pulse laser produced ion beam using a compact passive magnetic device. *Review of Scientific Instruments* 85, 043504.
- Chiari M, Migliori A and Mandò PA (2002) Investigation of beam-induced damage to ancient ceramics in external-PIXE measurements. *Nuclear Instruments and Methods in Physics Research Section B: Beam Interactions with Materials and Atoms* 188, 151–155.
- Crandall KR and Rusthoi DP (1997) *TSTEP* (Los Alamos National Laboratory Report LA-UR-97-886).
- Dromey B, Coughlan M, Senje L, Taylor M, Kuschel S, Villagomez-Bernabe B, Stefanuik R, Nersisyan G, Stella L, Kohanoff J, Borghesi M, Currell F, Riley D, Jung D, Wahlström C-G, Lewis CLS and Zepf M (2016) Picosecond metrology of laser-driven proton bursts. *Nature Communications* 7, 10642.
- Dunne M (2006) Applied physics: laser-driven particle accelerators. *Science* 312, 374–376.
- Eichner T, Grüner F, Becker S, Fuchs M, Habs D, Weingartner R, Schramm U, Backe H, Kunz P and Lauth W (2007) Miniature magnetic devices for laser-based, table-top free-electron lasers. *Physical Review Special Topics – Accelerators and Beams* 10, 082401.
- Ezeh GC, Obioh IB, Asubiojo OI, Chiari M, Nava S, Calzolari G, Lucarelli F and Nuviadenu C (2015) The complementarity of PIXE and PIGE techniques: a case study of size segregated airborne particulates collected from a Nigeria city. *Applied Radiation and Isotopes* 103, 82–92.
- Fourmaux S, Buffechoux S, Albertazzi B, Capelli D, Lévy A, Gnedyuk S, Lecherbourg L, Lassonde P, Payeur S, Antici P, Pépin H, Marjoribanks RS, Fuchs J and Kieffer JC (2013) Investigation of laser-driven proton acceleration using ultra-short, ultra-intense laser pulses. *Physics of Plasmas* 20, 013110.
- Fuchs J, Sentoku Y, Karsch S, Cobble J, Audebert P, Kemp A, Nikroo A, Antici P, Brambrink E, Blazevic A, Campbell EM, Fernández JC, Gauthier J-C, Geissel M, Hegelich M, Pépin H, Popescu H, Renard-LeGalloudec N, Roth M, Schreiber J, Stephens R and Cowan TE (2005) Comparison of laser ion acceleration from the front and rear surfaces of thin foils. *Physical Review Letters* 94, 045004.
- Giuntini L, Massi M and Calusi S (2007) The external scanning proton microprobe of Firenze: a comprehensive description. *Nuclear Instruments and Methods in Physics Research Section A: Accelerators, Spectrometers, Detectors and Associated Equipment* 576, 266–273.
- Grassi N, Migliori A, Mandò PA and Calvo del Castillo H (2005) Differential PIXE measurements for the stratigraphic analysis of the painting Madonna dei fusi by Leonardo da Vinci. *X-Ray Spectrometry* 34, 306–309.
- Green JS, Robinson APL, Booth N, Carroll DC, Dance RJ, Gray RJ, MacLellan DA, McKenna P, Murphy CD, Rusby D and Wilson L (2014) High efficiency proton beam generation through target thickness control in femtosecond laser-plasma interactions. *Applied Physics Letters* 104, 214101.
- Halbach K and Holsinger RF (1976) Superfish – a computer program for evaluation of RF cavities with cylindrical symmetry. *Particle Accelerators* 7, 213–222.
- Kar S, Ahmed H, Prasad R, Cerchez M, Brauckmann S, Aurand B, Cantono G, Hadjisolomou P, Lewis CLS, Macchi A, Nersisyan G, Robinson APL, Schroer AM, Swantusch M, Zepf M, Willi O and Borghesi M (2016) Guided post-acceleration of laser-driven ions by a miniature modular structure. *Nature Communications* 7, 10792.
- Kraft SD, Obst L, Metzkes-Ng J, Schlenvoigt H-P, Zeil K, Michaux S, Chatain D, Perin J-P, Chen SN and Fuchs J (2018) First demonstration of multi-MeV proton acceleration from a cryogenic hydrogen ribbon target. *Plasma Physics and Controlled Fusion* 60, 044010.
- Kühn S, Dumergue M, Kahaly S, Mondal S, Füle M, Csizmadia T, Farkas B, Major B, Várallyay Z, Cormier E, Kalashnikov M, Calegari F, Devetta M, Frassetto F, Månsson E, Poletto L, Stagera S, Vozzi C, Nisoli M, Rudawski P, Maclot S, Campi F, Wikmark H, Arnold CL, Hey CM, Johnsson P, L'Huillier A, Lopez-Martens R, Haessler S, Bocoum M, Boehle F, Vernier A, Iaquaniello G, Skantzakis E, Papadakis N, Kalpouzos C, Tzallas P, Lépine F, Charalambidis D, Varjú K, Osvey K and Sansone G (2017) The ELI-ALPS facility: the next generation of attosecond sources. *Journal of Physics B: Atomic, Molecular and Optical Physics* 50, 132002.
- Lazic V, Vadrucchi M, Fantoni R, Chiari M, Mazzinghi A and Gorghinian A (2018) Applications of laser-induced breakdown spectroscopy for cultural heritage: a comparison with X-ray fluorescence and particle induced X-ray emission techniques. *Spectrochimica Acta Part B: Atomic Spectroscopy* 149, 1–14.
- Macchi A (2017) A review of laser-plasma ion acceleration. Available at: <http://arxiv.org/abs/1712.06443>
- Malka V, Fritzier S, Lefebvre E, d'Humières E, Régis F, Grillon G, Albaret C, Meyroneinc S, Chambaret J-P, Antonetti A and Hulin D (2004) Practicability of protontherapy using compact laser systems. *Medical Physics* 31, 1587–1592.
- Mancic A, Robiche J, Antici P, Audebert P, Blancard C, Combis P, Dorchie F, Fausserier G, Fourmaux S, Harmande M, Kodama R,

- Lancia L, Mazevet S, Nakatsutsumi M, Peyrussee O, Recoules V, Renaudin P, Shepherd R and Fuchs J (2010) Isochoric heating of solids by laser-accelerated protons: experimental characterization and self-consistent hydrodynamic modeling. *High Energy Density Physics* **6**, 21–28.
- Mandò PA, Fedi ME and Grassi N (2011) The present role of small particle accelerators for the study of Cultural Heritage. *The European Physical Journal Plus* **126**, 41.
- Marteau F, Ghaith A, N'Gotta P, Benabderrahmane C, Valléau M, Kitegi C, Loulergue A, Vétéran J, Sebdaoui M, André T, Le Bec G, Chavanne J, Vallerand C, Oumbarek D, Cosson O, Forest F, Jivkov P, Lancelot JL and Couprie ME (2017) Variable high gradient permanent magnet quadrupole (QUAPEVA). *Applied Physics Letters* **111**, 253503.
- Masood U, Bussmann M, Cowan TE, Enghardt W, Karsch L, Kroll F, Schramm U and Pawelke J (2014) A compact solution for ion beam therapy with laser accelerated protons. *Applied Physics B* **117**, 41–52.
- Menu M, Calligaro T, Salomon J, Amsel G and Moulin J (1990) The dedicated accelerator-based IBA facility AGLAE at the Louvre. *Nuclear Instruments and Methods in Physics Research Section B: Beam Interactions with Materials and Atoms* **45**, 610–614.
- Migliorati M, Bacci A, Benedetti C, Chiadroni E, Ferrario M, Mostacci A, Palumbo L, Rossi AR, Serafini L and Antici P (2013) Intrinsic normalized emittance growth in laser-driven electron accelerators. *Physical Review Special Topics – Accelerators and Beams* **16**, 011302.
- Mondal S, Shirozhan M, Ahmed N, Bocoum M, Boehle F, Vernier A, Haessler S, Lopez-Martens R, Sylla F, Sire C, Quééré F, Nelissen K, Varjú K, Charalambidis D and Kahaly S (2018) Surface plasma attosource beam lines at ELI-ALPS. *Journal of the Optical Society of America B* **35**, A93.
- Morrison JT, Feister S, Frische KD, Austin DR, Ngirmang GK, Murphy NR, Orban C, Chowdhury EA and Roquemore WM (2018) Corrigendum: MeV proton acceleration at kHz repetition rate from ultra-intense laser liquid interaction (2018 New J. Phys. 20 022001). *New Journal of Physics* **20**, 069501.
- Nakamura S, Ikegami M, Iwashita Y, Shirai T, Tongu H, Souda H, Daido H, Mori M, Kado M, Sagisaka A, Ogura K, Nishiuchi M, Orimo S, Hayashi Y, Yogo A, Pirozhkov AS, Bulanov SV, Esirkepov T, Nagashima A, Kimura T, Tajima T, Takeuchi T, Fukumi A, Li Z and Noda A (2007) High-quality laser-produced proton beam realized by the application of a synchronous RF electric field. *Japanese Journal of Applied Physics* **46**, L717–L720.
- Nilsson H, Andersson J, Engström L, Lundberg H and Hartman H (2019) Experimental transition probabilities for 4p – 4d spectral lines in V II. *Astronomy & Astrophysics* **622**, A154.
- Nirkko M, Braccini S, Ereditato A, Kreslo I, Scamporrì P and Weber M (2013) An adjustable focusing system for a 2 MeV H<sup>+</sup> ion beam line based on permanent magnet quadrupoles. *Journal of Instrumentation* **8**, P02001.
- Nishiuchi M, Daito I, Ikegami M, Daido H, Mori M, Orimo S, Ogura K, Sagisaka A, Yogo A, Pirozhkov AS, Sugiyama H, Kiriya H, Okada H, Kanazawa S, Kondo S, Shimomura T, Tanoue M, Nakai Y, Sasao H, Wakai D, Sakaki H, Bolton P, Choi IW, Sung JH, Lee J, Oishi Y, Fujii T, Nemoto K, Souda H, Noda A, Iseki Y and Yoshiyuki T (2009) Focusing and spectral enhancement of a repetition-rated, laser-driven, divergent multi-MeV proton beam using permanent quadrupole magnets. *Applied Physics Letters* **94**, 061107.
- Passoni M, Fedeli L and Mirani F (2019) Superintense laser-driven ion beam analysis. *Scientific Reports* **9**, 9202.
- Patel PK, Mackinnon AJ, Key MH, Cowan TE, Foord ME, Allen M, Price DF, Ruhl H, Springer PT and Stephens R (2003) Isochoric heating of solid-density matter with an ultrafast proton beam. *Physical Review Letters* **91**, 125004.
- Pichon L, Calligaro T, Lemasson Q, Moignard B and Pacheco C (2015) Programs for visualization, handling and quantification of PIXE maps at the AGLAE facility. *Nuclear Instruments and Methods in Physics Research Section B: Beam Interactions with Materials and Atoms* **363**, 48–54.
- Radepon M, Lemasson Q, Pichon L, Moignard B and Pacheco C (2018) Towards a sharpest interpretation of analytical results by assessing the uncertainty of PIXE/RBS data at the AGLAE facility. *Measurement* **114**, 501–507.
- Re A, Angelici D, Giudice AL, Corsi J, Allegretti S, Biondi AF, Gariani G, Calusi S, Gelli N, Giuntini L, Massi M, Taccetti F, La Torre L, Rigato V and Pratesi G (2015) Ion beam analysis for the provenance attribution of lapis lazuli used in glyptic art: the case of the “Collezione Medicea”. *Nuclear Instruments and Methods in Physics Research Section B: Beam Interactions with Materials and Atoms* **348**, 278–284.
- Romano F, Schillaci F, Cirrone GAP, Cuttone G, Scuderi V, Allegra L, Amato A, Amico A, Candiano G, De Luca G, Gallo G, Giordanengo S, Fanola Guarachi L, Korn G, Larosa G, Leanza R, Manna R, Marchese V, Marchetto F, Margarone D, Milluzzo G, Petringa G, Pipek J, Pulvirenti S, Rizzo D, Sacchi R, Salamone S, Sedita M and Vignati A (2016) The ELIMED transport and dosimetry beam line for laser-driven ion beams. *Nuclear Instruments and Methods in Physics Research Section A: Accelerators, Spectrometers, Detectors and Associated Equipment* **829**, 153–158.
- Roso L (2018) High repetition rate Petawatt lasers. *EPJ Web of Conferences* **167**, 01001.
- Santos HC, Pappalardo CCL, Catalano R, Orlando A and Romano FRFP (2016) Identification of forgeries in historical enamels by combining the non-destructive scanning XRF imaging and alpha-PIXE portable techniques. *Microchemical Journal* **124**, 241–246.
- Schollmeier M, Becker S, Geißel M, Flippo KA, Blažević A, Gaillard SA, Gautier DC, Grüner F, Harres K, Kimmel M, Nürnberg F, Rambo P, Schramm U, Schreiber J, Schüttrumpf J, Schwarz J, Tahir NA, Atherton B, Habs D, Hegelich BM and Roth M (2008) Controlled transport and focusing of laser-accelerated protons with miniature magnetic devices. *Physical Review Letters* **101**, 055004.
- Schreiner M, Melcher M and Uhlir K (2007) Scanning electron microscopy and energy dispersive analysis: applications in the field of cultural heritage. *Analytical and Bioanalytical Chemistry* **387**, 737–747.
- Scisciò M, Migliorati M, Palumbo L and Antici P (2018) Design and optimization of a compact laser-driven proton beam line. *Scientific Reports* **8**, 6299. doi:10.1038/s41598-018-24391-2
- Scuderi V, Bijan Jia S, Carpinelli M, Cirrone GAP, Cuttone G, Korn G, Licciardello T, Maggiore M, Margarone D, Pisciotta P, Romanof B, Schillaci F, Stancampiano C and Tramontana A (2014) Development of an energy selector system for laser-driven proton beam applications. *Nuclear Instruments and Methods in Physics Research Section A: Accelerators, Spectrometers, Detectors and Associated Equipment* **740**, 87–93.
- Sharma A (2018) High energy electron and proton acceleration by circularly polarized laser pulse from near critical density hydrogen gas target. *Scientific Reports* **8**, 2191.
- Sharma A, Tibai Z, Hebling J and Fülöp JA (2018) Quasi-monoenergetic proton acceleration from cryogenic hydrogen microjet by ultrashort ultraintense laser pulses. *Physics of Plasmas* **25**, 033111.
- Sorieul S, Alfauert P, Daudin L, Serani L and Moretto P (2014) Aifira: an ion beam facility for multidisciplinary research. *Nuclear Instruments and Methods in Physics Research Section B: Beam Interactions with Materials and Atoms* **332**, 68–73.
- Ter-Avetisyan S, Schnürer M, Polster R, Nickles PV and Sandner W (2008) First demonstration of collimation and monochromatisation of a laser accelerated proton burst. *Laser and Particle Beams* **26**, 637–642.
- Vallières S, Puyuelo-Valdes P, Salvadori M, Bienvenue C, Payeur S, d'Humières E and Antici P (2019) The laser-driven ion acceleration beam line on the ALLS 200 TW for testing nanowire targets. In Esarey E, Schroeder CB and Schreiber J (eds), *Laser Acceleration of Electrons, Protons, and Ions V*, SPIE, p. 2. <http://spie.org/Publications/Proceedings/Paper/10.1117/12.2520178>
- Wilks SC, Krueer WL, Tabak M and Langdon AB (1992) Absorption of ultra-intense laser pulses. *Physical Review Letters* **69**, 1383–1386.
- Young LM (1996) TRACE3D. (LANL Report LA-UR-96-1835).
- Zucchiatti A and Agulló-Lopez F (2012) Potential consequences of ion beam analysis on objects from our cultural heritage: an appraisal. *Nuclear Instruments and Methods in Physics Research, Section B: Beam Interactions with Materials and Atoms* **278**, 106–114.
- Zucchiatti A and Redondo-Cubero A (2014) Ion beam analysis: new trends and challenges. *Nuclear Instruments and Methods in Physics Research, Section B: Beam Interactions with Materials and Atoms* **331**, 48–54.